3D BIOPRINTING OF ANISOTROPIC ENGINEERED TISSUE CONSTRUCTS WITH ULTRASONICALLY INDUCED CELL PATTERNING

Parth Chansoria
Edward P. Fitts Department of Industrial and Systems Engineering, North Carolina State University, Raleigh, NC 27695, US

Comparative Medicine Institute, North Carolina State University, Raleigh, NC 27695, US

Rohan Shirwaiker[1]
Edward P. Fitts Department of Industrial and Systems Engineering, North Carolina State University, Raleigh, NC 27695, US

Comparative Medicine Institute, North Carolina State University, Raleigh, NC 27695, US

Joint Department of Biomedical Engineering, North Carolina State University and University of North Carolina at Chapel Hill, Raleigh, NC 27695, US

ABSTRACT

As 3D bioprinting continues to evolve as a promising alternative to engineer complex human tissues in-vitro, there is a need to augment bioprinting processes to achieve the requisite cellular and extracellular organizational characteristics found in the original tissues. While the cell distribution within bioinks is typically homogeneous, incorporating appropriate cellular patterning within the bioprinted constructs is an essential first step towards the eventual formation of anisotropically organized tissue matrix essential to its biomechanical form and function. This study describes a new bioprinting technique that uses ultrasonic standing bulk acoustic waves (SBAW) to organize cells into controllable anisotropic patterns within viscous bioinks while maintaining high cell viability. First, we develop a 3D computational model to discern the SBAW pressure pattern in response to multiple ultrasonic frequencies (0.71 – 2 MHz). We then experimentally analyze the patterns and viabilities of human adipose-derived stem cells (hASC) and human osteosarcoma cells (MG63) in alginate as a function of the SBAW frequency. Computational results indicate the formation of parallel pressure strands with higher pressure amplitudes near the bottom of the deposited layer, which is corroborated by experimental images of cell patterning. The inter-strand spacing is found to be affected by the frequency ($p < 0.0001$), while an interaction effect between the cell type and frequency governs the width of the strands ($p = 0.02$). Further, we demonstrate the synergistic bioprinting and SBAW-induced patterning of hASC within alginate and gelatin methacrylate (GelMA) constructs in tandem with chemical and photo-crosslinking, respectively. Pertinent cellular patterning and viability of at least 80% were noted in the alginate and GelMA constructs across the experimental design space. Finally, we demonstrate the vat photo-polymerization-based bioprinting of a 3-layered GelMA construct with hASC strand lay pattern of 0-45-90° across the layers. This work represents a step forward in advancing bioprinting capabilities to achieve biomimetic tissue constructs.

Keywords: bioprinting, ultrasound, biomimicry, standing bulk acoustic wave (SBAW), alginate, GelMA

1. INTRODUCTION

The anisotropic distribution of cellular and extra-cellular components plays a vital role in the functionality of most mammalian tissues. For example, cardiac muscle tissue consists of cardiomyocytes with striated myofibrils that withstand the expansive and contractile forces associated with cardiac cycle [1,2]. Such organizational characteristics are also evident in musculoskeletal tissues, such as the linear arrangement of elongated fibroblastic cells and collagen fibrils in ligaments and tendons that impart an enhanced capability to withstand tensile loads [3,4] and crisscross fibrous organization in annulus fibrosus that disperses the associated intervertebral loads [5].

Since the last two decades, tissue engineering (TE) technologies are being developed to create tissues, in vitro, for clinical and diagnostic applications [6,7]. In these technologies, achieving the appropriate cellular patterning, as a precursor to achieving the desired extra-cellular matrix (ECM) organization, is essential to replicate the functionality of the engineered tissues and their relevance to practical applications. This is supported by studies using micro-architectures of fibrous polymer scaffolds as structural cues to guide cells and the subsequent formation of organized ECM [8,9]. Lately, bioprinting has gained increased interest in augmenting the capabilities of TE for complex tissue fabrication [10,11]. Bioprinting involves the computer-aided deposition or curing of cell-laden biomaterials (bioinks) in a layer-wise fashion. In addition to being able to mimic the macro-geometry of the native tissues, it allows for precise placement of different cell-types, materials and growth factors, which enables fabrication of complex tissues such as heart [12,13] and liver [14,15]. However, the intrinsic homogeneity of cell distribution within the bioinks can be a limiting factor in achieving the relevant micro-architectural organizational characteristics within the bioprinted constructs. Of note, recent investigations on narrow strands of high cell densities indicate that the associated

[1] Contact author: rashirwaiker@ncsu.edu

intercellular signaling can result in aligned ECM formation [16]. In the context of bioprinting, stimulating the formation of appropriately organized network of cells within the deposited bulk layers of the construct can promote the formation of well-organized ECM network, thereby leading to a significant advancement towards biomimicry. Accordingly, this study focuses on the development of a bioprinting process that utilizes ultrasonic standing bulk acoustic waves (SBAW) to organize cells into parallel strands of high cellular densities within single or multi-layered viscous hydrogels. According to literature, pulsed ultrasound under optimized intensities can be non-deleterious to cells, and in fact, can promote cell proliferation and ECM production [17,18]. As such, ultrasound is already being used in the medical domain for physiotherapy [19,20] and imaging [21,22]. In recent years, ultrasonic standing surface acoustic waves (SSAW) have been explored to manipulate or pattern cells. However, these efforts have primarily been in micro-fluidic systems [23–25] and low viscosity fluids. SSAW approaches utilize standing waves within the substrate to drive cell alignment and rely on acoustic streaming for 3D manipulation of individual cells across limited distances (in the order of micrometers) [26]. This limits their translation to bioprinting wherein, typically, the bioinks are viscous, the engineered tissue constructs are thick (in the order of millimeters), and bulk cellular manipulation is required. In contrast, the SBAW approach in this study creates longitudinal standing waves within the bulk of the bioink through laterally generated pressure waves. As such, the SBAW-driven process mechanics is virtually independent of the number of layers or their thicknesses, and hence, better-suited for 3D bioprinting. Moreover, the SBAW approach can use off the shelf components and be modulated for achieving unique cellular patterns, unlike the relatively more expensive and rigid substrate and fabrication requirements in SSAW approaches.

This study describes the new bioprinting approach and relationships between the SBAW frequency, cell organizational patterns, and cell viability determined via 3D multi-physics computational modeling and designed experiments with two types of cells (human adipose-derived stem cells (hASC) and human osteosarcoma cells (MG63)) within chemically-crosslinkable alginate and photo-crosslinkable gelatin methacrylate (GelMA) hydrogels. The vat photo-polymerization-based bioprinting of a multi-layered GelMA construct with cellular strands oriented in a 0-45-90° lay pattern across layers is also demonstrated to highlight the layer-wise control offered by the process and its versatility.

2. THEORY

Fig. 1 illustrates the process of using ultrasound to pattern cells along parallel strands within the bioink. The process utilizes an ultrasonic patterning fixture (UPF) that consists of an electroacoustic transducer and an opposing rigid reflector inside a hollow encasing. The bioink (fluid matrix with cells) is deposited within the hollow encasing, and the transducer is excited via a sinusoidal high frequency voltage signal. This excitation is in the form of ultrasonic frequency vibrations that create a longitudinal bulk acoustic pressure wave in the fluid. This pressure variation can be expressed as a combination of complex harmonic terms [27]:

$$p(x,t) = Ae^{i\omega(t-x/c)} + Be^{i\omega(t+x/c)} \quad (1)$$

where, i is an imaginary number, ω is the angular frequency ($\omega = 2\pi f$, where f is the ultrasonic frequency) and c is the speed of sound in the bioink. In Eq. (1), the first and second term with their associated scalar coefficients (A and B) represent pressure waves travelling in the positive and negative x-direction (emitted and reflected waves, respectively), with p(x,t) being the resulting interference. A and B can be solved for using the boundary conditions of spatially non-varying pressure at the transducer end (x = 0) and a zero spatial pressure gradient at the reflective end (x = L) [27]:

$$p(0,t) = P_0 e^{i\omega t} \quad (2)$$

$$\partial p/\partial x \text{ (at } x = L) = 0 \quad (3)$$

where P_0 is the pressure amplitude. Solving these boundary conditions results in the SBAW with pressure varying only along the x-axis (since the transducer excitation is along the x-axis), given by [28]:

$$p(x,t) = P_0 \cos(\omega t)\cos(\omega x/c) \quad (4)$$

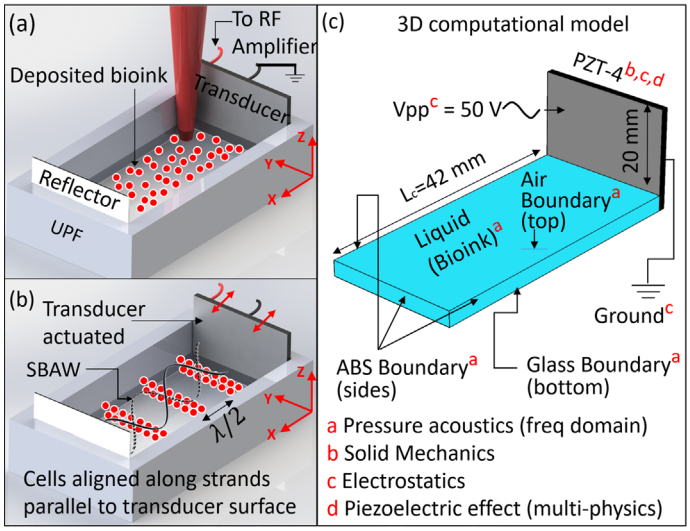

Fig. 1. (a) Ultrasonic patterning fixture (UPF) for patterning cells in viscous bioinks. (b) The SBAW pressure variation within the UPF exerts radiation force on the cells to arrange them along straight strands. (c) Setup of the 3D linear acoustic model of the top view of the UPF illustrating the multi-physics interfaces in COMSOL.

The nodes of this pressure variation are planes parallel to the transducer-reflector surfaces and are spaced out by λ/2, where λ is the ultrasound wavelength (c/f). Eq. (4) is followed up with a

boundary condition on the transducer-reflector distance given by:

$$L_{SW} = n\lambda/2 \quad (5)$$

where n (an integer) denotes the number of pressure nodes. This imposes a design constraint on the UPF, wherein L_{SW} needs to be an integer multiple of half the wavelength for a successful formation of SBAW. For speed of sound in bioink (c ~1500 m/s), an L_{SW} of 42 mm suffices the design constraint for the four frequencies that will be computationally and experimentally investigated in this work (0.71, 1, 1.5, 2 MHz). Once the SBAW is created, the resulting acoustic radiation force (ARF) exerted on the cells suspended in the bioink causes them to traverse and arrange at the nearest pressure nodes. This force is given by [28,29]:

$$ARF = (\pi/3c)(k_s-k_c)r^3\omega P_0^2 \sin(2\omega x/c) \quad (6)$$

where k_s and k_c are the compressibility of bioink and cell, respectively, and r is the cell radius. From Eq. (6), it is evident that the ARF would increase by increasing the frequency, pressure amplitude, and the radius of the cell. In viscous bioinks, the movement of a cell towards the nearest pressure node due to the ARF would be slowed down by viscous drag force (DF) from the bioink, given by:

$$DF = 6\pi\eta r v \quad (7)$$

where η is the dynamic viscosity of the bioink and v is the instantaneous velocity of the cell. Greater ARF amplitude would increase the rate of movement of the cells, thereby increasing the DF [30]. This may increase the shear forces on the cells, in turn, affecting their viability.

3. MATERIALS AND METHODS

3.1 Ultrasonic patterning fixture (UPF) and auxiliary apparatus

The UPF encasing was 3D printed out of acrylonitrile butadiene styrene (uPrint SE Plus, Stratasys, MN) and attached onto a glass substrate using a biocompatible glue (MG30, Infinity Bond Adhesives). The same glue was then used to attach an electroacoustic transducer (piezo-ceramic plate type, SM 111 material, Steiner & Martins Inc, FL) as the wave generating surface and a glass cover slip (BRAND®, Millipore Sigma, Burlington, MA) as the rigid reflective surface on opposite ends of the encasing. The sinusoidal voltage signal to excite the transducers was generated from a function generator (Keysight Technologies Inc., CA) and amplified from an RF amplifier (Electronics & Innovation Ltd., NY).

3.2 3D Computational model in COMSOL to determine SBAW pressure variation

To determine the pressure variation patterns and amplitudes, which would subsequently govern the corresponding cellular patterns and viability characteristics, a 3D finite element analysis (FEA) model was formulated in the Acoustic-Piezoelectric interaction interface in COMSOL Multiphysics® (Comsol Inc., MA). The interfaces were setup as per Fig. 1(c). To the liquid domain, to accurately model the propagation of the pressure wave and formation of SBAW, a conservative estimate of frequency-dependent attenuation of ultrasound (α in dB/m) in alginate-gelatin based hydrogels was applied as [31]:

$$\alpha = 12f \quad (8)$$

To the boundaries of the liquid domain not contacting the transducer, a material dependent acoustic impedance (Z_m) was assigned as:

$$Z_m = \rho_m c_m \quad (9)$$

where ρ_m is the density of the medium that the hydrogel bioink is in contact with at that boundary, and c_m is the speed of sound in that medium. These boundaries constituted 3D printed ABS at the sides ($\rho_{m(ABS)}$ = 1070 kg/m^3 and $c_{m(ABS)}$ = 2230 m/s), glass at the bottom ($\rho_{m(glass)}$ = 8000 kg/m^3 and $c_{m(glass)}$ = 4540 m/s) and air at the top ($\rho_{m(air)}$ = 1.22 kg/m^3 and $c_{m(air)}$ = 343 m/s).

In the solid mechanics and electrostatics interfaces, manufacturer-defined compliance attributes were assigned to model the deformation characteristics of the electroacoustic transducer. These included an isotropic structural loss factor of 1/1800, a dielectric dissipation factor of 0.4, and coefficients of the stiffness matrix (c_E) and coupling matrix (e^T) of $c_{E(11)} = c_{E(22)}$ = 86 GPa, $c_{E(33)}$ = 73 GPa, $c_{E(66)}$ = 172 GPa, and $e^T_{(31)} = e^T_{(32)}$ = -12.4 C/m^2, $e^T_{(33)}$ = 23.36 C/m^2, respectively, in the stress charge form of transducer compliance:

$$T = c_E S + e^T E \quad (10)$$

where T is the stress exhibited by the transducers, and S and E are the strain and applied electric field, respectively. To the transducer surface contacting the bioink, a harmonic perturbation having voltage amplitude of 25 V was applied, while the other surface was grounded. A fixed constraint was also applied to the transducer at the grounded surface. For the entire model, at each frequency (0.71, 1, 1.5, 2 MHz), a mapped rectangular mesh with maximum element size of 0.03 mm (< $\lambda/10$ at each transducer frequency) was used to achieve convergence [32]. The model was computed for four separate 3D setups, each having transducer thickness dependent on the resonant frequency as per the manufacturer specifications. On a desktop computer with 32 GB of RAM and 16 GB of dedicated graphics, the computation for each geometry with approximately 4.5×10^6 degrees of freedom lasted approximately 13 minutes.

3.3 Bioink preparation

To prepare the cells, cryopreserved hASC (R7788115, Thermo Fisher Scientific, MA) or MG63 (CRL®-1427™, ATCC, VA) were plated in T-75 flasks (Nunc™ Easy Flask™, Thermo Fisher Scientific). The hASC were proliferated in MesenPro RS basal media with growth supplement (Thermo Fisher Scientific) and

1% L-Glutamine (Thermo Fisher Scientific). The MG63 cell media comprised of 90% v/v minimum essential medium without L-glutamine (MilliporeSigma, MA) and 10% v/v fetal bovine serum (Thermo Fisher Scientific). The T-75 flasks were incubated at 37°C and 5% CO_2 with media changes on alternate days until 80% confluency.

The cells used for the first set of experiments to study patterning characteristics in alginate were stained using neutral red dye (MilliporeSigma). These cells were incubated in 5 ml of filter sterilized cell growth media supplemented with 5 mg of dye for 45 min. The cells were then harvested using TrypLE Express enzyme (Gibco, Thermo Fisher Scientific) and spun at 100 g for 5 min to form a cell pellet.

For the set of experiments to analyze cell viability via Live/Dead® assay 3 h post-bioprinting, the cells were not stained with neutral-red dye, since this dye would have confounded the results of the viability assay by labeling all viable cells fluorescent in the red emission spectra.

The alginate matrix constituted a 2% w/v solution of high molecular weight alginate powder (Manugel® GMB, DuPont, DE) in PBS (MilliporeSigma). After adding the powder to PBS, the solution was rigorously vortexed for 10 s, sonicated for 5 min, and then autoclaved at 121°C and 16 psi for 30 min to form the sterile alginate matrix ($\eta \sim 70$ cP). It was then stored at 37°C until further experiments.

The GelMA matrix ($\eta \sim 30$ cP at 37°C) comprised of 5% w/v sterile GelMA containing 0.25% w/v LAP (Lithium phenyl-2,4,6-trimethylbenzoylphosphinate) photo-initiator (CELLINK, Gothenburg, Sweden). The GelMA was stored at 4°C until the day of the experiment and equilibrated at 37°C for 30 min prior to the bioink preparation.

To formulate the bioinks, the supernatant media atop the cell pellet was gently aspirated, followed by addition of appropriate volumes of alginate or GelMA solutions. The bioinks were constituted with a concentration of 1 million cells/ml using gentle pipetting.

3.4 Characterizing the cellular patterns in alginate in response to different ultrasonic frequencies

In the first study, we characterized the progression of cellular patterning over time in alginate first because it is more viscous of the two bioinks, and successful patterning in alginate would ensure patterning in GelMA. Towards this, three separate UPFs were made for each frequency group to organize the neutral-red stained cells and assess two patterning characteristics – inter-strand spacing and strand width. During these experiments, the UPFs were filled with 4 ml of PBS and kept on the imaging platform with bottom illumination within a dissection microscope (EZ4, Leica Microsystems, Germany). 1 ml of the bioink was subsequently deposited and allowed to disperse for 30 s. A sinusoidal voltage signal with amplitude of 25 V, applied in intermittent bursts of 1 s with 1 s pauses, was applied to the transducer to create well-defined cellular strands within 1 min of excitation at each of the four frequencies for each of the two cell types. Top view images were captured at 0 s (time of commencement transducer excitation) and 60 s. From the images captured at 60 s, inter-cellular strand spacing and strand width were measured using custom MATLAB (Mathworks, MA) scripts [33]. Briefly, the script required the user to define the bounding boxes around the cellular strands. Then, a contrast-based algorithm identified the pixels corresponding to neutral-red stained cells and calculated the inter-strand spacing as the distance between the centroids of the detected pixels in adjacent strands. The strand-width was calculated as the maximum horizontal distance between the detected pixels within each bounding box. For each frequency and cell type, the inter-strand spacing and strand widths were determined at three randomly selected locations per image from three images per sample for three independently fabricated samples (i.e., n = 27 data points per group).

3.5 Synergistic bioprinting, SBAW-assisted patterning, and crosslinking of single layered alginate and GelMA constructs

After characterizing the fundamental patterning characteristics based on variations in ultrasonic frequency and cell type, we investigated the persistence of the patterns and cell viability in 3D cellular constructs following synergistic bioprinting, ultrasonically-induced patterning, and bioink crosslinking in the second study. The alginate and GelMA constructs were bioprinted in a commercial bioprinter (CELLINK) and crosslinked via chemical- and photo-crosslinking methods, respectively, at the four aforementioned frequencies. These experiments were performed using hASC-based bioinks, since these non-cancerous cells are being extensively utilized for therapeutic tissue engineering research and applications [34–36].

In preparation for bioprinting, the UPF was setup on the bioprinter build platform, and 3 ml of the bioink (alginate or GelMA) was loaded into a 3 ml syringe extruder cartridge (BioX, CELLINK). Another 10 ml cartridge was filled with 4 ml of filter sterilized 1% w/v $CaCl_2$ in PBS to be used for crosslinking the alginate. A 22G nozzle (inner Ø = 0.72 mm) was attached to the bioink cartridge, while a 30G nozzle (inner Ø = 0.16 mm) was used for the low viscosity crosslinker.

To fabricate the alginate constructs, 2 ml of bioink (at 37°C) was printed into UPF pre-filled with 4 ml of PBS as adjacent strands in a 20 x 40 mm geometry at an extrusion pressure of 3 kPa and print speed of 10 mm/s. In tandem, the transducer was actuated by a 25 V sinusoidal voltage signal in bursts of 1 s followed by 1 s pauses. This was commensurate with the outcomes of the previous patterning study. The burst mode of excitation especially helped to minimize the impedance heating of the transducer and any deleterious effects thereof. After 1 min of excitation, 4 ml of the crosslinker was printed into the UPF at the rate of 1 ml/min achieved through an extrusion pressure of 16 kPa and print speed of 10 mm/s. The presence of PBS in the fixture during crosslinking ensured uniform dispersion of the Ca^{2+} gelation ions. The transducer excitation was maintained for 5 min during the progression of crosslinking (15 min), which enabled the retention of organized cells within the bioink. After 15 min of crosslinking, the construct was retrieved from the

fixture using flat-headed forceps and subject to further assessment.

The general bioprinting protocol for GelMA constructs was similar, except that the fixtures were not pre-filled with PBS, and UV exposure was used instead of $CaCl_2$ to crosslink the constructs. Briefly, 2 ml of bioink at 37 °C was printed into the UPF at an extrusion pressure of 2 kPa and print speed of 10 mm/s, followed by excitation of the transducer (25 V sinusoidal voltage with 1 s bursts). After 1 min of excitation, the bioink was crosslinked by exposure to 405 nm UV, with a separation of 50 mm (40 mW/cm^2 UV intensity) between the in-built UV LED and the dispensed bioink. The transducer excitation was switched off after 5 min while the UV exposure was allowed to continue up to 15 min, and the crosslinked construct was retrieved using flat headed forceps. The average thickness of the alginate and GelMA constructs was 2.5 mm (Video 1).

The constructs containing neutral-red stained cells were imaged using a DSLR camera (EOS 80D, Canon, Japan). The constructs containing non-neutral-red stained cells (n = 3 per group) were gently transferred to a 100 mm petri dish and incubated in 10 ml culture media for 3 h. This step was necessary to ensure that the cells were able to recover from prior processing steps before analyzing their viability. After 3 h, the viability assessment was performed using Live/Dead assay (Life Technologies, CA). Herein, the media was aspirated followed by addition of 2 ml of PBS containing 4 µl EthD-I and 1 µl calcein AM over the constructs. The constructs were then incubated for 30 min, and each construct was subsequently imaged at three randomly-selected locations using a fluorescent microscope (DM5500B, Leica Microsystems, Germany). The corresponding average % cell viability was determined for each group based on image analyses of live (green emission spectra) and dead (red emission spectra) cells using a custom MATLAB script.

3.6 Bioprinting multi-layered GelMA construct with 0-45-90° cellular strand lay orientation

To demonstrate the versatility of the ultrasound-patterning approach, we created a UPF variant by attaching three 2 MHz transducer-reflector pairs on a petri dish such that the pairs were angled relative to each other in increments of 45°. Therefore, if one pair was assigned the orientation 0°, the other pairs had orientation of 45° and 90°, respectively. A corresponding L_{SW} of 54 mm was used to satisfy Eq. (5) and successfully induce the SBAW. The transducers were excited via high frequency relays (G6K 2P RF, Omron Electronics LLC, IL) controlled by a microcontroller (Arduino Uno) that switched on the relevant relay, thereby exciting the corresponding transducer, as per the orientation required for a particular layer. This setup was utilized to bioprint a 3-layered GelMA construct via vat photo-polymerization, with cellular strands oriented along 0°, 45° and 90° in the three layers, respectively.

To estimate the characteristics of cellular patterns in this setup prior to the experiment, a 2D linear-acoustic computational model of the top view of the UPF with the three transducer-reflector pairs was setup in COMSOL. A 3D model similar to the one described previously was highly computationally intensive, and hence not practical. In the 2D model, the transducer compliance characteristics were the same as those used in section 3.2, while the outer edges of the liquid (hydrogel) domain were assigned a sound hard boundary condition. A free tetrahedral mesh of maximum element size of 0.03 mm was used to achieve convergence. With 2×10^7 degrees of freedom, the solver computed the solution in approximately 35 min.

To fabricate the construct, first, 5 ml of GelMA bioink (1 million neutral-red stained hASC/ml) at 37°C was deposited into the UPF, resulting in a layer height of 1.5 mm. Transducer #1 was then excited at 25 V amplitude in burst mode, and the cells were allowed to organize for 1 min. A 405 nm 100 mW UV laser (405MD-100-1445, Q-Baihe) was subsequently traversed at 2 mm/s at a height of 30 mm above the GelMA layer to selectively crosslink a 20×20 mm^2 construct with hASC organized and entrapped along the 0° orientation. Similarly, 5 ml of GelMA was deposited for layers 2 and 3, and transducers #2 and #3 actuated, respectively, with subsequent selective crosslinking to create the layers with cells organized and entrapped along 45° and 90° orientation, respectively. The overall construct dimensions, therefore, were 20×20×4.5 mm^3. The neighboring uncrosslinked bioink was then aspirated and the construct carefully extracted using flat-headed forceps for further imaging.

3.7 Statistical analysis

Two-way ANOVA and Tukey post-hoc tests were used to assess the effects of frequency (0.71, 1, 1.5 and 2 MHz) and cell type (hASC and MG63) on the patterning characteristics (inter-strand spacing and strand width) of cells in alginate (n = 3 per group) in the first study. Similarly, two-way ANOVA and Tukey post-hoc tests were used to assess the effects of frequency (0.71, 1, 1.5 and 2 MHz) and bioink type (alginate, GelMA) on the viability of the patterned hASC (n = 3 per group) in the bioprinted crosslinked constructs in the second study. All tests were performed in JMP® (SAS, Cary, NC) and statistical significance assessed at $\alpha = 0.05$.

4. RESULTS AND DISCUSSION

4.1 Computational outcomes

The computational results of variation of acoustic pressure in the UPF with respect to frequency are shown in Fig. 2. Whereas the pressure nodes manifest as uniform planes parallel to the transducer surface in theory, the computational results highlighted a pressure distribution pattern varying across the depth of the fluid, with larger pressure amplitudes at the bottom of the fixture, and almost zero pressure near the top. To better visualize this pressure distribution, two separate sections were taken – one along the x-z plane at the center of the UPF and another at the bottom of the UPF along the x-y plane. The pressure distribution in the bottom view (x-y plane) depicted straight nodal lines in accordance with the theory. The peak pressure amplitudes followed a non-linear relationship with respect to the frequency in decreasing order for 1.5 MHz (29.7 kPa), 2 MHz (22.4 kPa), 1 MHz (20.2 kPa), and 0.71 MHz (11.6 kPa), respectively.

At the boundaries of the fluid domain, a portion of the pressure wave emanating from the transducer (p_i) gets reflected back into the fluid. The pressure of this reflected wave (p_r) can be given as:

$$p_r(x,t) = p_i(x,t)(Z_m - Z_f)/(Z_m + Z_f) \quad (11)$$

where Z_f is the acoustic impedance of fluid, which in this case is the hydrogel bioink ($\rho_f \sim 1015$ kg/m^3 and $c_f = 1500$ m/s). At the air-liquid boundary in the computational model, the acoustic impedance of air is negligible compared to that of liquid ($Z_{m(air)} << Z_f$), which leads to an almost 180° out of phase reflection of the incident pressure wave [37] as per Eq. (11). The resulting interference yields the zero-pressure region at the top of the fluid domain (near the air-liquid boundary).

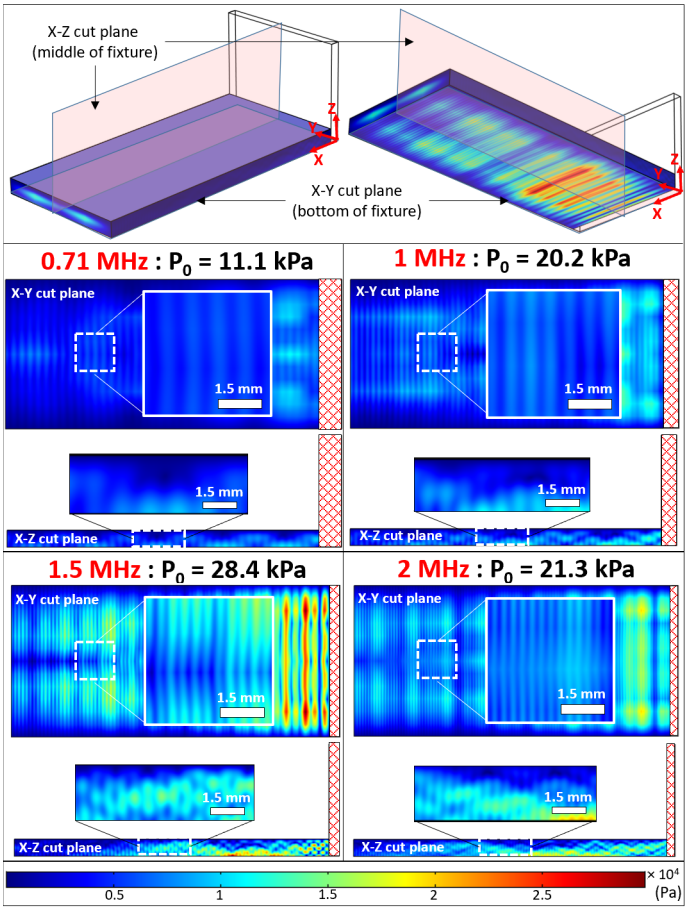

Fig. 2. Acoustic pressure distribution in UPF as seen in 3D (top panel) and corresponding cut sections along x-y and x-z planes for analysis. Pressure distribution pattern along the x-y section (bottom view) depicts straight nodal lines at each frequency in accordance with the theory. The x-z sectional view elucidates the non-uniform pressure distribution along the depth of the fluid, with greater radiation pressures estimated near the glass bottom of the fixture. The relationship between frequency and pressure amplitude was non-linear, with the highest amplitude noted at 1.5 MHz and lowest at 0.71 MHz. In each fixture, the red-hatched pattern denotes the transducer, which had different thickness specific to each resonant frequency.

It should be noted that the values above are calculated for attenuation of ultrasound in alginate-gelatin bioink, which is at least an order of magnitude greater (12 dB/m at 1 MHz) than that in water (0.43 dB/m at 1 MHz [38]). When the model is analyzed at 2 MHz (highest frequency in the experimental design, the difference between the maximum SBAW pressure P_0 between water (22.4 kPa) and bioink (21.3 kPa) is minimal. This is because the length scales are too small to be able to observe a large pressure difference. Therefore, as long as the length scales are relatively small, the bioink-specific attenuation of ultrasound will have less impact on the resulting SBAW pressure variation.

4.2 hASC and MG63 patterning characteristics in alginate solution as a function of ultrasonic frequency

Upon application of the sinusoidal voltage signal, the resulting SBAW due to transducer vibration gradually patterned the cells at their nearest pressure nodes to form cellular strands. The progression of hASC patterning over 60 s is evident in Fig. 3(b). Although the pressure amplitude at 0.71 MHz was approximately an order of magnitude less than that at 1.5 MHz, distinct and measurable cellular patterning was observed after 60 s of actuation, nonetheless. Fig. 3 (c-f) depicts the patterns at each frequency after 60 s.

Output of MATLAB analysis of the inter-cellular strand spacing is illustrated in Fig. 4(a). As per results of the two-way ANOVA, the inter-strand spacing was significantly affected by the frequency ($p < 0.0001$), and not by the cell type ($p = 0.98$) or their interaction ($p = 0.058$). Post-hoc results indicate that the spacing at each frequency was independent of the cell type, but for each cell type, spacing at each frequency was significantly different ($p < 0.01$). The spacings also closely correlated with the theoretical spacing ($\lambda/2$), which is indicative of a high degree of controllability of the spatial distribution of the cells by altering the ultrasonic frequency.

The results of the measured strand width are presented in Fig. 4(b). Results of two-way ANOVA show a significant interaction effect of cell type and frequency on the strand width ($p = 0.02$). Corresponding estimates for strand width were highest at 0.71 MHz, which can be attributed to the smaller acoustic pressures at that frequency and a greater distance of traversal from the pressure antinode to the nearest node ($\lambda/4$) in the SBAW. The estimates of the widths were lower at 1.5 and 2 MHz on account of the higher acoustic pressure (at 1.5 MHz) and smaller traversal distance between the antinode and the nearest node (at 2 MHz). Comparing between hASC and MG63 cells, it is evident that the strand width was different between the two cell types only at 0.71 MHz ($p = 0.013$). Herein, the relatively smaller strand width with hASC can be attributed to its comparatively larger cell radius, which results in these cells traversing and clustering faster due to higher radiation force. As per Eqs. (6) and (7) and literature [30], the increase in radiation force due to increase in radius is higher (ARF $\propto r^3$) than the corresponding increase in the drag force (DF $\propto$ r), thereby resulting in smaller patterning times.

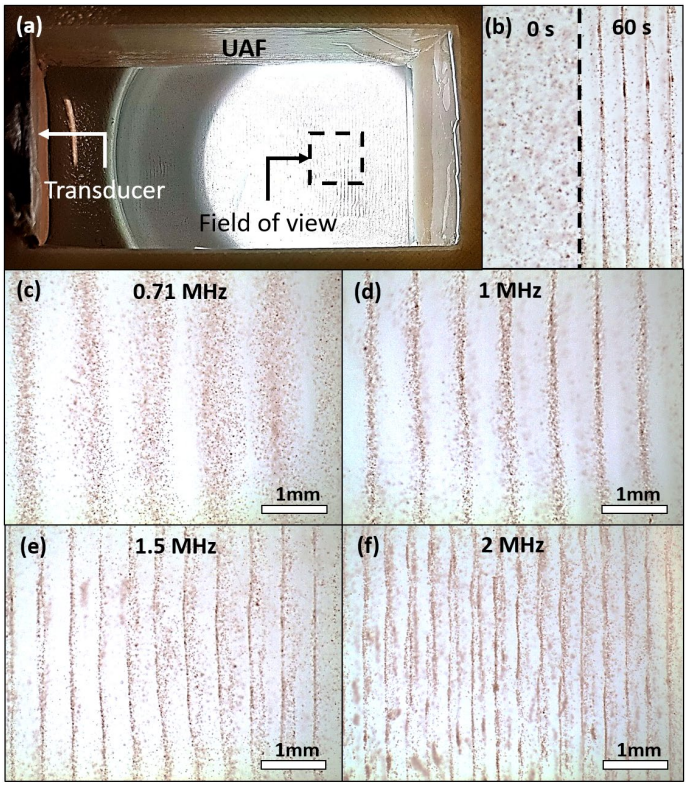

Fig. 3. (a) Top view of UPF at 2 MHz. (b) Patterning of hASC in alginate over 60 s in the 2 MHz fixture. (c-f) hASC patterned within alginate at SBAW frequencies of 0.71, 1, 1.5, and 2 MHz, respectively, after 60 s of actuation. The patterning characteristics of MG63 cells were similar to those of hASC.

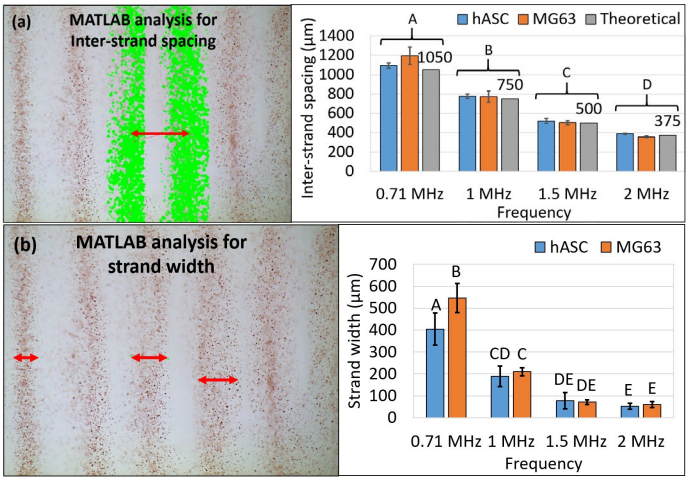

Fig. 4. (a) Representative example of MATLAB image analysis to determine inter-strand spacing based on centroid-centroid distance of adjacent strands of clustered cells (left), and corresponding results (right), which indicate a significant effect of frequency ($p < 0.0001$) on the spacing. The spacing at each frequency was closely correlated with the theoretical spacing ($\lambda/2$), irrespective of the cell type. (b) Representative example of MATLAB image analysis to determine strand width as the distance between the extremities of individual strands of clustered cells (left), and corresponding results (right), which indicate a significant effect of the interaction of frequency and cell type ($p = 0.02$) on the spacing. Letters A-D denote statistically significant post-hoc differences ($p < 0.01$).

At any given cell concentration in the bioink, larger strand width would denote less dense packaging of the cells within their respective strands. A lesser cell density within individual strands may lead to an unorganized ECM formation due to the lack of relevant inter-cellular signaling cues [39]. Towards this, smaller widths could be achieved by increasing the pressure amplitude (by increasing the voltage amplitude to the transducer). This could, however, increase the radiation pressure (and hence ARF), which would, in turn, increase the viscous drag on the cells, possibly affecting their viability. Another alternative for reducing the strand width would be to allow cells more time to traverse to the nodes by delaying the time of introduction of the crosslinking mechanism. However, an important nuance to highlight here is that too much delay in crosslinking initiation may cause the cells to settle down towards the bottom of the layer in their respective strands due to gravity, resulting in the loss of three-dimensionality of cellular patterning (cells organized across parallel planes). Therefore, a synergy of computational modeling and experiments, similar to the one described in this study, could be used to pre-determine the pressure amplitudes that are non-deleterious to the cells, and that would still result in cellular patterning across each layer, with large enough cell densities (smaller width) to induce organized ECM throughout the layer.

In conjunction with the strand width, it is important to allow sufficient gap between the strands to minimize cells within adjacent strands from bridging the gap and producing unorganized ECM fibers [40]. The gap, however, cannot be too large or the ECM fibers will be too far apart, resulting in poor mechanical characteristics. Since the gap between the strands is a function of both inter-strand spacing and the strand width, it could be controlled by controlling the SBAW frequency (to control the inter-strand spacing), and its combination with the pressure amplitude and crosslinker initiation delay (to control the strand width). Such effects of the interplay of strand width and inter-strand spacing towards tissue-specific ECM organization will be investigated in future studies.

4.3 hASC patterning characteristics and viability in crosslinked alginate and GelMA constructs

Fig. 5 demonstrates the entrapping of patterned neutral red stained hASC within chemically crosslinked and photo-crosslinked constructs of alginate and GelMA fabricated via synergistic bioprinting and SBAW-assisted patterning. Since the neutral red dye selectively stains live cells, exhibition of redness in the cells post-bioprinting is indicative of the non-deleteriousness of the process.

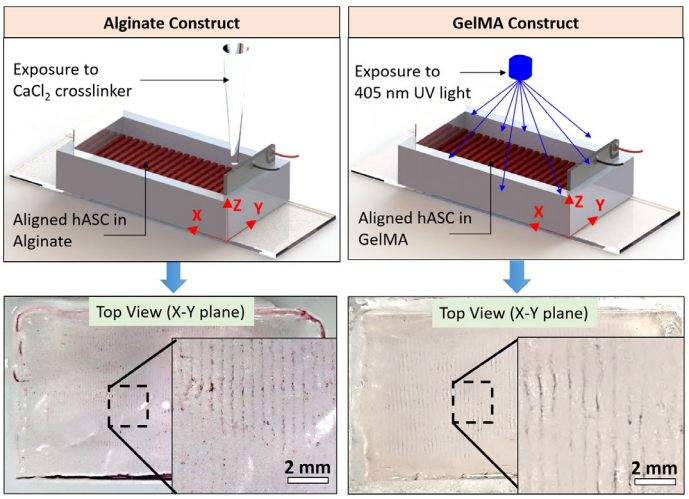

Fig. 5. Crosslinking methods involving exposure to $CaCl_2$ or 405 nm UV light to crosslink Alginate or GelMA, respectively. The corresponding crosslinked constructs depict preservation of cellular patterns across the macro-geometry of the constructs.

Representative live/dead images from the viability analysis of crosslinked constructs of both bioinks are shown in Fig. 6. Recall that the hASC used in this subset of experiments were not neutral-red stained. A viability of 100% was noted in all GelMA groups, while the viability of the alginate groups varied from 80 – 100%. Results of two-way ANOVA show a significant effect of the interaction of bioink type and frequency ($p < 0.0001$) on the hASC viability. Post hoc tests within alginate indicate that the viability at 1 MHz was significantly lower than that of the other three groups. Furthermore, the viability at 0.71 MHz and 1.5 MHz were also significantly different than that at 2 MHz. To explain this non-linear trend of viability, three key factors can be considered – acoustic cavitation effects, fluid streaming-induced perturbations, and shear forces on the cells due to the viscous drag. Cavitation occurs when dissolved gas bubbles expand and collapse during the transducer excitation bursts, thereby creating localized surge in temperature and pressure, which has been demonstrated to rupture cell membranes [41]. These effects are higher at lower frequencies and higher pressure amplitudes [42]. Streaming-induced perturbations occur when the transducer deformation is non-uniform across its surface due to manufacturing defects, thereby creating differences in acoustic pressures within the contacting fluid. These effects are higher at moderate frequencies and may cause vortexing effects that may be deleterious to the cells [43]. Lastly, larger radiation force acting on the cells increases their speed of migration to the node, thereby increasing the viscous drag and hence the shear forces on their cell membranes. These shear forces would be more enhanced for more viscous bioinks such as alginate than GelMA, resulting in comparatively lower viability at some frequencies. Across the four frequencies in alginate, the reduced viability at 0.71 MHz could be primarily attributed to the increased cavitation effects. The 1 MHz group exhibited higher radiation pressures than 0.71 MHz and thus could have been more susceptible to cavitation effects. Moreover, this group also exhibited increased streaming-induced perturbations, which, coupled with the effect of cavitation, could explain the lowest observed viability. Finally, the 1.5 MHz group was associated with the highest radiation forces (due to highest radiation pressures) and therefore increased shear forces on the migrating cells which may have lowered their viability. Nevertheless, a viability of at least 80% is acceptable for tissue engineering applications, and it could potentially improve if the constructs are matured further under appropriate culture conditions.

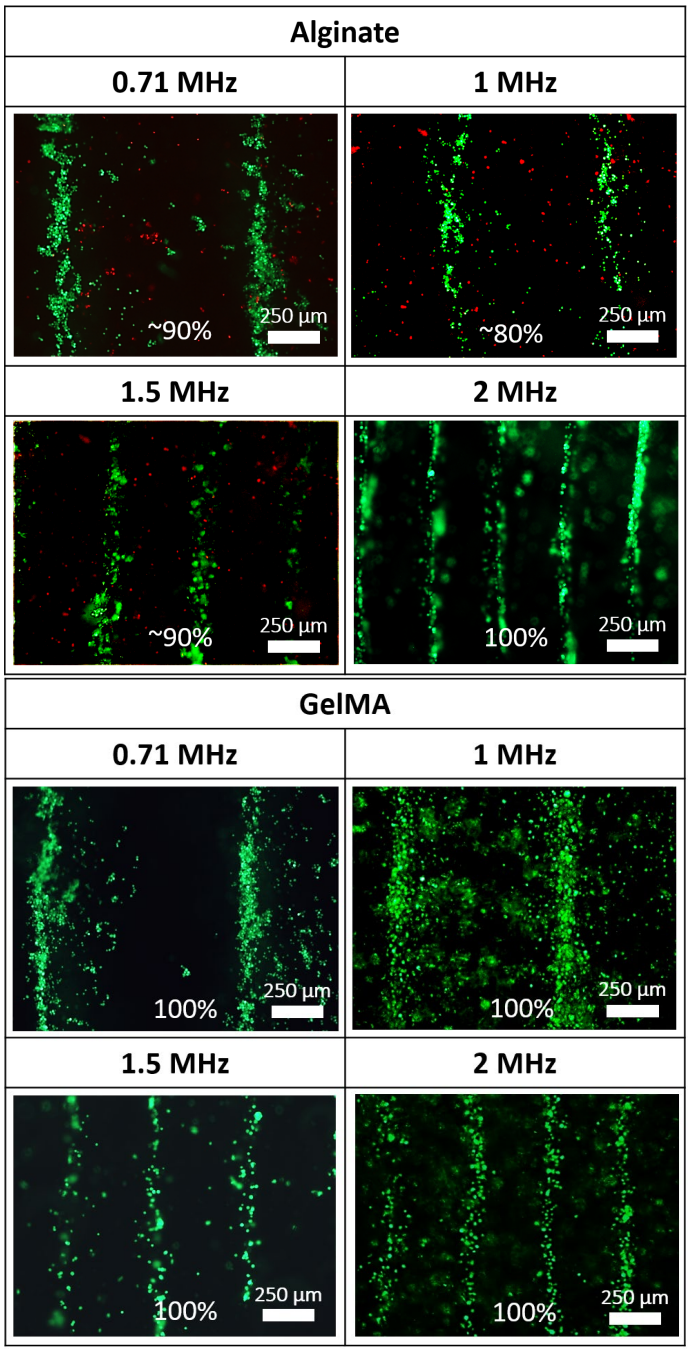

Fig. 6. Representative Live/Dead® images of cells patterned within crosslinked Alginate and GelMA constructs, wherein a

significant effect of the interaction of bioink type and frequency ($p < 0.0001$) was noted. The selected UAB parameters resulted in constructs with hASC viability of at least 80%, which is relevant for tissue engineering applications.

To further improve the viability in the alginate groups that demonstrated less than 100% viability, the key will be to reduce the acoustic radiation pressure acting on the cells, thereby reducing their speed of traversal to the node and the corresponding drag forces acting on them, as well as the cavitation effects. This could primarily be achieved by reducing the voltage amplitude to actuate the transducer. However, note that there will be a practical lower limit on the voltage amplitude to still achieve cell patterning. This will be the voltage amplitude at which the acoustic radiation forces are large enough to result in reasonable patterning times as per the process and application. For example, for a voltage amplitude lower than 25 Vpp, initiation of the crosslinking would have to be deferred by more than the 1 min interval used in this work. To further improve viability, cavitation effects could also be lowered by use of surfactants [42], or by smaller actuation bursts to prevent large bubble formation in the bioinks [42]. To prevent fluid streaming-induced perturbations, custom-made transducers with more uniform surface deformation (compliance) characteristics could be developed.

Representative live/dead images of the side views are shown in Fig. 7. In both alginate and GelMA constructs, the cell density in the patterned strands can be noted to be higher in the bottom regions, closer to the substrate. This is in agreement with results of the computational model, wherein the radiation pressure diminishes towards the top of the constructs due to the air-liquid interface. Nevertheless, the overall pattern depicts cellular strands as parallel planes, which shall be difficult to achieve in a SSAW-based patterning that uses substrate vibrations for cellular manipulation.

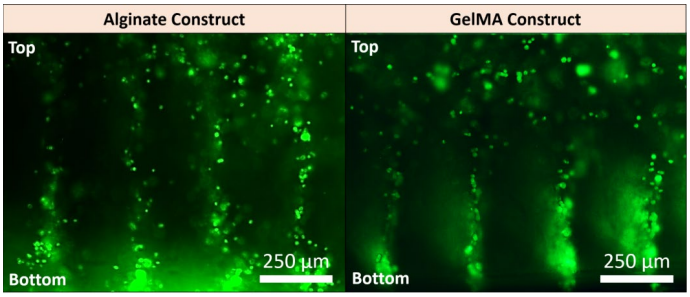

Fig. 6. Representative Live/Dead® images of the side views (x-z cut plane) of the alginate and GelMA constructs at 2 MHz. The patterning characteristics of the alginate and GelMA constructs are commensurate with the computational model, wherein a higher density of cell organization within the arrays was evident near the substrate. The patterning characteristics at other frequencies were similar.

Although this study has shown creation of thick (2.5 mm) constructs relevant for applications such as engineered ligaments and tendons, the process can also be used for patterning cells within thinner constructs. This is because the pressure wave is propagated laterally (along the x-axis in Fig. 1(b)) into the bioink upon vibration of the transducer. As long as the deformational characteristics of the transducer are uniform across its wave-generating surface, the SBAW can be created and the cells organized within the bioink, independent of the layer thickness.

4.4 Bioprinted multi-layer construct with 0-45-90° hASC orientation

Fig. 8(a) illustrates the vat photopolymerization-based 3D bioprinting of the three-layered construct with horizontal (0°), inclined (45°) and vertical (90°) cell orientation in layers 1-3, respectively. Within each layer, the cells were patterned and subsequently entrapped via crosslinking in linear strand patterns parallel to the transducer being actuated. The results of the 2D computational model (Fig. 8(b)) demonstrated the pressure nodal lines (and hence the cell orientation) within a layer to be parallel to the transducer being actuated. The 405 nm UV laser selectively crosslinked a 20×20 mm^2 GelMA construct (Fig. 8(c,d)) that lied between each of the transducer-reflector pairs. Fig. 8(e) depicts the microscopic images highlighting distinct cellular patterning along each orientation (0°, 45°, 90°) across the three layers with the same reference coordinate system. Such patterns are relevant towards several anisotropic tissues such as ligaments and tendons, which have cells and ECM predominantly organized in a linear fashion [3], or more complex tissues such as annulus fibrosus [3] or heart muscle [44] that consist of crisscross or interspersed cellular and ECM organization. It can also be noted that more complex patterns such as circular (or circumferential) could be created by changing the shape of the transducer or reflector surface or changing their position in real-time to alter the cell patterning characteristics across the tissue geometry. We are currently investigating such strategies.

5. CONCLUSIONS AND FUTURE WORK

This work investigated the capabilities of a process that uses ultrasonic SBAW to organize multiple cell types within multiple types of bioinks. It also demonstrated the integration of the SBAW-assisted patterning approach with bioprinting processes based on extrusion and vat photopolymerization principles. While other fundamentally different techniques for cell patterning such as electrophoresis [47,48], magnetophoresis [49,50], photophoresis [51,52] or chemotaxis [53,54] exist, unlike the label-free [55] and contact-less [56] approach of SBAW-assisted cell manipulation, these techniques may require chemical or magnetic labeling, or complex and expensive apparatus which may not be integrable with bioprinting. Moreover, the fundamental mechanics to get parallel organization of cells within the entirety of the viscous bioinks would be very complex to model with these techniques, whereas the mechanics of SBAW-assisted cell patterning is straightforward and can provide repeatable results.

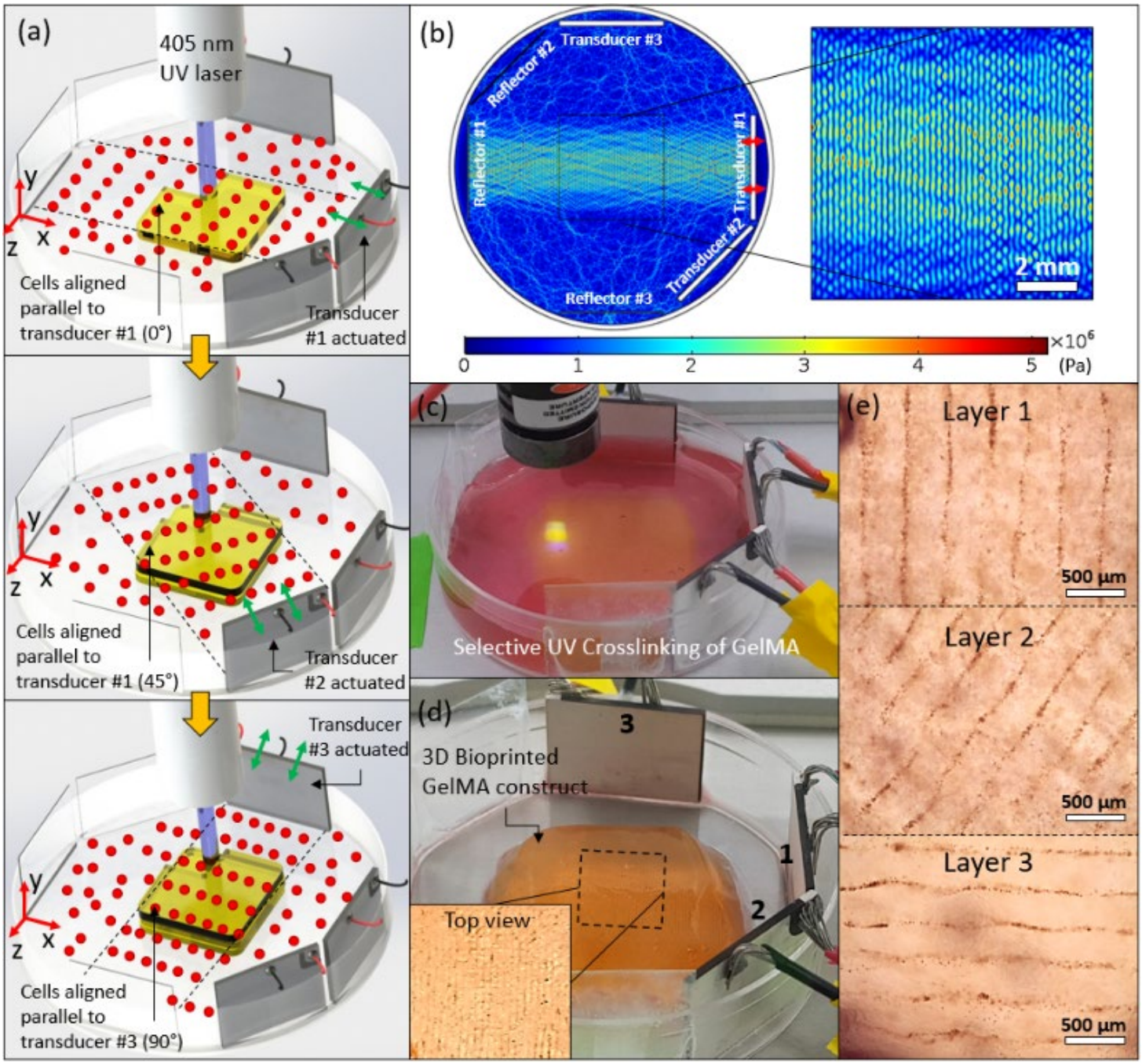

Fig. 7. 3D bioprinting of 3 layered GelMA construct with 0°-45°-90° cell orientation. (a) Actuation of transducer#1 after deposition of first layer of bioink orients the cells along the horizontally (0° : parallel to x-axis). Subsequent crosslinking using the UV laser crosslinks the GelMA solution into a hydrogel with entrapped cells in the 0° orientation. Similarly, deposition of layers 2 and 3 and associated transducer actuation and photopolymerization entraps the cells in 45° (45° relative to x-axis) and 90° (parallel to z-axis) orientation across the two layers. (b) Acoustic pressure distribution for the first layer of bioink within the UAF as seen from the top, which depicts nodal lines parallel to the actuated transducer. Pressure distribution in layers 2 and 3 depicts nodal lines parallel to transducer 2 and 3. (c) Selective UV crosslinking to create the bioprinted GelMA construct in (d). The inset in the top view depicts the overlapping cell orientations (e) Microscopic brightfield images depicting 0°-45°-90° organizational pattern across layers 1-3, respectively.

The process takes place within a custom-made UPF consisting of opposing transducer-reflector pairs, wherein the transducer vibration at ultrasonic frequencies creates the SBAW to exert radiation forces on the cells to pattern them. The 3D computational model highlighted the acoustic pressure variations in the UPF as a pattern consisting of parallel nodal planes with greater pressure amplitudes near the bottom of the bioink layer. Experimental studies demonstrated cellular patterning along straight strands at the pressure nodal planes, with greater degree of cell patterning near the bottom of the constructs, which is in accordance with the computational model outcomes. The spacing between adjacent cell strands was governed only by the frequency and not the cell type, highlighting that repeatable patterns can be created by just altering the frequency. The strand width was dependent on the transducer frequency and cell type, and the experimental values were in agreement with the corresponding analytical and computational estimates. Furthermore, within the bioprinted constructs containing patterned cells within alginate and GelMA bioinks, the resultant cell viability was at least 80%, which further highlights the adequacy of this process for tissue engineering applications. Lastly, a 3-layered GelMA construct with 0-45-90° cell orientation in each layer was fabricated, thereby asserting the flexibility of this approach to fabricate complex cellular architectures.

Future studies shall focus on assessing functional characteristics of cells (e.g., alignment/morphology within the patterns, phenotype, ECM formation, gene expression) in culture over time. For such longer term in vitro culture studies, especially for alginate, peptide modifications of its polymeric chains may be necessary to stimulate more favorable cellular responses [45,46]. In general, using a higher viscosity bioink would necessitate the re-optimization of process parameters and crosslinking protocol to entrap the cellular patterns within the construct. In this case, while using higher voltage amplitudes would increase the pressure amplitude, thereby increasing the ARF to achieve quicker patterning, this could adversely affect the cell viability. At the same time, greater straining of the transducer at higher voltage amplitudes could also induce undesired turbulence due to acoustic streaming and distort the cell patterns. The advised strategy is to use lower voltages coupled with a slower crosslinking protocol, similar to the one described in this work, to alleviate the streaming issue while achieving three-dimensional cellular patterning and higher viability. In general, altering the voltage amplitude would not affect the spacing between adjacent cellular strands, as this is dependent only on the applied ultrasound wavelength. However, changes in bioink viscosity might alter the spacing due to different speed of sound at the same frequency. As such, a thorough understanding and optimization of the material and process parameters is required to achieve high fidelity of cellular patterns and high cell viability in the bioprinted constructs relevant to the tissue application.

Future studies will also focus on the optimization of cell concentrations, layer height, strand width and inter-strand spacing, layer-wise patterning orientations and UAB parameters to achieve appropriate ECM responses and biomechanical properties using tissue-specific cells to develop various important tissues including ligaments, tendons and the knee meniscus.

6. ACKNOWLEDGEMENTS

We would like to acknowledge support from the US NSF (CMMI#1652489) and NVIDIA (GPU grant). We would also like to disclose that a PCT application has been filed for the technology described herein (PCT/US19/56859).

7. REFERENCES

[1] J.W. Buikema, P. Van Der Meer, J.P.G. Sluijter, I.J. Domian, Concise Review: Engineering Myocardial Tissue: The Convergence of Stem Cells Biology and Tissue Engineering Technology, Stem Cells. 31 (2013) 2587–2598. doi:10.1002/stem.1467.

[2] P.P. Purslow, The Extracellular Matrix of Skeletal and Cardiac Muscle, in: Collagen, Springer US, Boston, MA, 2008: pp. 325–357. doi:10.1007/978-0-387-73906-9_12.

[3] R.L. Mauck, B.M. Baker, N.L. Nerurkar, J.A. Burdick, W.-J. Li, R.S. Tuan, D.M. Elliott, Engineering on the Straight and Narrow: The Mechanics of Nanofibrous Assemblies for Fiber-Reinforced Tissue Regeneration, Tissue Eng. Part B Rev. 15 (2009) 171–193. doi:10.1089/ten.teb.2008.0652.

[4] H.L. Birch, C.T. Thorpe, A.P. Rumian, Specialisation of extracellular matrix for function in tendons and ligaments., Muscles. Ligaments Tendons J. 3 (2013) 12–22. doi:10.11138/mltj/2013.3.1.012.

[5] A. Baldit, Micromechanics of the Intervertebral Disk, Multiscale Biomech. (2018) 455–467. doi:10.1016/B978-1-78548-208-3.50011-3.

[6] R. Langer, J.P. Vacanti, Tissue engineering, Science. 260 (1993) 920–926.

[7] F.J. O'Brien, Biomaterials & scaffolds for tissue engineering, Mater. Today. 14 (2011) 88–95. doi:10.1016/S1369-7021(11)70058-X.

[8] P.B. Warren, P. Huebner, J.T. Spang, R.A. Shirwaiker, M.B. Fisher, Engineering 3D-Bioplotted scaffolds to induce aligned extracellular matrix deposition for musculoskeletal soft tissue replacement, Connect. Tissue Res. 58 (2017) 342–354. doi:10.1080/03008207.2016.1276177.

[9] C.H. Lee, H.J. Shin, I.H. Cho, Y.-M. Kang, I.A. Kim, K.-D. Park, J.-W. Shin, Nanofiber alignment and direction of mechanical strain affect the ECM production of human ACL fibroblast, Biomaterials. 26 (2005) 1261–1270. doi:10.1016/J.BIOMATERIALS.2004.04.037.

[10] B. Starly, R.A. Shirwaiker, Three-dimensional Bioprinting, in: L. Zhang, J.P. Fisher, K. Leong (Eds.), 3D Bioprinting Nanotechnol. Tissue Eng. Regen. Med., Academic Press, Waltham, 2015: pp. 57–77.

[11] S. V Murphy, A. Atala, 3D bioprinting of tissues and

organs, Nat. Biotechnol. 32 (2014) 773–785. doi:10.1038/nbt.2958.

[12] W.-H. Zimmermann, I. Melnychenko, T. Eschenhagen, Engineered heart tissue for regeneration of diseased hearts, Biomaterials. 25 (2004) 1639–1647. doi:10.1016/S0142-9612(03)00521-0.

[13] T.C. Flanagan, B. Wilkins, A. Black, S. Jockenhoevel, T.J. Smith, A.S. Pandit, A collagen-glycosaminoglycan co-culture model for heart valve tissue engineering applications, Biomaterials. 27 (2006) 2233–2246. doi:10.1016/J.BIOMATERIALS.2005.10.031.

[14] S.F. Badylak, D. Taylor, K. Uygun, Whole-organ tissue engineering: decellularization and recellularization of three-dimensional matrix scaffolds., Annu. Rev. Biomed. Eng. 13 (2011) 27–53. doi:10.1146/annurev-bioeng-071910-124743.

[15] R.N.B. Bhandari, L.A. Riccalton, A.L. Lewis, J.R. Fry, A.H. Hammond, S.J.B. Tendler, K.M. Shakesheff, Liver Tissue Engineering: A Role for Co-culture Systems in Modifying Hepatocyte Function and Viability, Tissue Eng. 7 (2001) 345–357. doi:10.1089/10763270152044206.

[16] H. Aubin, J.W. Nichol, C.B. Hutson, H. Bae, A.L. Sieminski, D.M. Cropek, P. Akhyari, A. Khademhosseini, Directed 3D cell alignment and elongation in microengineered hydrogels, Biomaterials. 31 (2010) 6941–6951. doi:10.1016/J.BIOMATERIALS.2010.05.056.

[17] T. Takayama, N. Suzuki, K. Ikeda, T. Shimada, A. Suzuki, M. Maeno, K. Otsuka, K. Ito, Low-intensity pulsed ultrasound stimulates osteogenic differentiation in ROS 17/2.8 cells, Life Sci. 80 (2007) 965–971. doi:10.1016/J.LFS.2006.11.037.

[18] A. RAMIREZ, J.A. SCHWANE, C. McFARLAND, B. STARCHER, The effect of ultrasound on collagen synthesis and fibroblast proliferationin vitro, Med. &amp Sci. Sport. &amp Exerc. 29 (1997) 326–332. doi:10.1097/00005768-199703000-00007.

[19] M.K. Patrick, Ultrasound in physiotherapy, Ultrasonics. 4 (1966) 10–14. doi:10.1016/0041-624X(66)90002-3.

[20] S.J. Warden, J.M. McMeeken, Ultrasound usage and dosage in sports physiotherapy, Ultrasound Med. Biol. 28 (2002) 1075–1080. doi:10.1016/S0301-5629(02)00552-5.

[21] J.W. Hunt, M. Arditi, F.S. Foster, Ultrasound Transducers for Pulse-Echo Medical Imaging, IEEE Trans. Biomed. Eng. BME-30 (1983) 453–481. doi:10.1109/TBME.1983.325150.

[22] T.A. Ritter, T.R. Shrout, R. Tutwiler, K.K. Shung, A 30-MHz piezo-composite ultrasound array for medical imaging applications, IEEE Trans. Ultrason. Ferroelectr. Freq. Control. 49 (2002) 217–230. doi:10.1109/58.985706.

[23] A. Barani, H. Paktinat, M. Janmaleki, A. Mohammadi, P. Mosaddegh, A. Fadaei-Tehrani, A. Sanati-Nezhad, Microfluidic integrated acoustic waving for manipulation of cells and molecules, Biosens. Bioelectron. 85 (2016) 714–725. doi:10.1016/J.BIOS.2016.05.059.

[24] Y. Qiu, H. Wang, C.E.M. Demore, D.A. Hughes, P. Glynne-Jones, S. Gebhardt, A. Bolhovitins, R. Poltarjonoks, K. Weijer, A. Schönecker, M. Hill, S. Cochran, Acoustic devices for particle and cell manipulation and sensing., Sensors (Basel). 14 (2014) 14806–38. doi:10.3390/s140814806.

[25] J. Friend, L.Y. Yeo, Microscale acoustofluidics: Microfluidics driven via acoustics and ultrasonics, Rev. Mod. Phys. 83 (2011) 647–704. doi:10.1103/RevModPhys.83.647.

[26] F. Guo, Z. Mao, Y. Chen, Z. Xie, J.P. Lata, P. Li, L. Ren, J. Liu, J. Yang, M. Dao, S. Suresh, T.J. Huang, Three-dimensional manipulation of single cells using surface acoustic waves., Proc. Natl. Acad. Sci. U. S. A. 113 (2016) 1522–7. doi:10.1073/pnas.1524813113.

[27] L.E. Kinsler, Fundamentals of acoustics, Wiley, 2000. http://adsabs.harvard.edu/abs/1999fuac.book.....K (accessed December 21, 2018).

[28] K. Yosioka, Y. Kawasima, Acoustic radiation pressure on a compressible sphere, Acta Acust. United with Acust. 5 (1955) 167–173. https://www.ingentaconnect.com/content/dav/aaua/1955/00000005/00000003/art00004 (accessed October 9, 2018).

[29] M. Settnes, H. Bruus, Forces acting on a small particle in an acoustical field in a viscous fluid, Phys. Rev. E. 85 (2012) 016327. doi:10.1103/PhysRevE.85.016327.

[30] R. Barnkob, P. Augustsson, T. Laurell, H. Bruus, Measuring the local pressure amplitude in microchannel acoustophoresis, Lab Chip. 10 (2010) 563. doi:10.1039/b920376a.

[31] Bush NL, Hill CR., Gelatine-alginate complex gel: a new acoustically tissue-equivalent material., Ultrasound Med. Biol. (1983).

[32] M.-S. Scholz, B.W. Drinkwater, T.M. Llewellyn-Jones, R.S. Trask, Counterpropagating wave acoustic particle manipulation device for the effective manufacture of composite materials, IEEE Trans. Ultrason. Ferroelectr. Freq. Control. 62 (2015) 1845–1855. doi:10.1109/TUFFC.2015.007116.

[33] P. Chansoria, L.K. Narayanan, K. Schuchard, R.A. Shirwaiker, Ultrasound-assisted biofabrication and bioprinting of preferentially aligned three-dimensional cellular constructs, Biofabrication. (2019). doi:10.1088/1758-5090/ab15cf.

[34] L.K. Narayanan, P. Huebner, M.B. Fisher, J.T. Spang, B. Starly, R.A. Shirwaiker, 3D-Bioprinting of Polylactic Acid (PLA) Nanofiber–Alginate Hydrogel Bioink Containing Human Adipose-Derived Stem Cells, ACS Biomater. Sci. Eng. 2 (2016) 1732–1742. doi:10.1021/acsbiomaterials.6b00196.

[35] L.F. Mellor, M. Mohiti-Asli, J. Williams, A. Kannan, M.R. Dent, F. Guilak, E.G. Loboa, Extracellular Calcium

Modulates Chondrogenic and Osteogenic Differentiation of Human Adipose-Derived Stem Cells: A Novel Approach for Osteochondral Tissue Engineering Using a Single Stem Cell Source., Tissue Eng. Part A. 21 (2015) 2323–33. doi:10.1089/ten.TEA.2014.0572.

[36] I.F. Cengiz, H. Pereira, L. de Girolamo, M. Cucchiarini, J. Espregueira-Mendes, R.L. Reis, J.M. Oliveira, Orthopaedic regenerative tissue engineering en route to the holy grail: disequilibrium between the demand and the supply in the operating room., J. Exp. Orthop. 5 (2018) 14. doi:10.1186/s40634-018-0133-9.

[37] P. Morse, K. Ingard, Theoretical acoustics, 1986. https://books.google.com/books?hl=en&lr=&id=KIL4MV9IE5kC&oi=fnd&pg=PR7&dq=P.+M.+Morse+and+K.+U.+Ingard,+Theoretical+Acoustics+(Princeton+University+Press,+Princeton,+NJ,+1986)&ots=hlMhD6MhH1&sig=EGtQj2rLa1V0hmiSOI9PXluTjQc (accessed December 21, 2018).

[38] J. Slotwinski, Ultrasonics Testing, in: L. Mordfin (Ed.), Handb. Ref. Data Nondestruct. Test., ASTM International, West Conshohocken, 2002: pp. 31–48.

[39] H. Aubin, J.W. Nichol, C.B. Hutson, H. Bae, A.L. Sieminski, D.M. Cropek, P. Akhyari, A. Khademhosseini, Directed 3D cell alignment and elongation in microengineered hydrogels, Biomaterials. 31 (2010) 6941–6951. doi:10.1016/J.BIOMATERIALS.2010.05.056.

[40] Y. Sun, R. Duffy, A. Lee, A.W. Feinberg, Optimizing the structure and contractility of engineered skeletal muscle thin films, Acta Biomater. 9 (2013) 7885–7894. doi:10.1016/J.ACTBIO.2013.04.036.

[41] R.K. Schlicher, H. Radhakrishna, T.P. Tolentino, R.P. Apkarian, V. Zarnitsyn, M.R. Prausnitz, Mechanism of intracellular delivery by acoustic cavitation, Ultrasound Med. Biol. 32 (2006) 915–924. doi:10.1016/J.ULTRASMEDBIO.2006.02.1416.

[42] M. Ashokkumar, The characterization of acoustic cavitation bubbles – An overview, Ultrason. Sonochem. 18 (2011) 864–872. doi:10.1016/J.ULTSONCH.2010.11.016.

[43] P. Chansoria, L.K. Narayanan, K. Schuchard, R.A. Shirwaiker, Ultrasound-assisted biofabrication and bioprinting of preferentially aligned three-dimensional cellular constructs, Biofabrication. (2019). doi:10.1088/1758-5090/ab15cf.

[44] R. Avazmohammadi, J.S. Soares, D.S. Li, S.S. Raut, R.C. Gorman, M.S. Sacks, A Contemporary Look at Biomechanical Models of Myocardium, Annu. Rev. Biomed. Eng. 21 (2019) 417–442. doi:10.1146/annurev-bioeng-062117-121129.

[45] J. Yu, K.T. Du, Q. Fang, Y. Gu, S.S. Mihardja, R.E. Sievers, J.C. Wu, R.J. Lee, The use of human mesenchymal stem cells encapsulated in RGD modified alginate microspheres in the repair of myocardial infarction in the rat, Biomaterials. 31 (2010) 7012–7020. doi:10.1016/J.BIOMATERIALS.2010.05.078.

[46] M. Shachar, O. Tsur-Gang, T. Dvir, J. Leor, S. Cohen, The effect of immobilized RGD peptide in alginate scaffolds on cardiac tissue engineering, Acta Biomater. 7 (2011) 152–162. doi:10.1016/J.ACTBIO.2010.07.034.

[47] K. Park, H.-J. Suk, D. Akin, R. Bashir, Dielectrophoresis-based cell manipulation using electrodes on a reusable printed circuit board, Lab Chip. 9 (2009) 2224. doi:10.1039/b904328d.

[48] T.P. Hunt, R.M. Westervelt, Dielectrophoresis tweezers for single cell manipulation, Biomed. Microdevices. 8 (2006) 227–230. doi:10.1007/s10544-006-8170-z.

[49] W. Liu, N. Dechev, I.G. Foulds, R. Burke, A. Parameswaran, E.J. Park, A novel permalloy based magnetic single cell micro array, Lab Chip. 9 (2009) 2381. doi:10.1039/b821044f.

[50] T. Kimura, Y. Sato, F. Kimura, M. Iwasaka, S. Ueno, Micropatterning of Cells Using Modulated Magnetic Fields, Langmuir. 21 (2005) 830–832. doi:10.1021/LA047517Z.

[51] R.K. Pirlo, Z. Ma, A. Sweeney, H. Liu, J.X. Yun, X. Peng, X. Yuan, G.X. Guo, B.Z. Gao, Laser-guided cell micropatterning system, Rev. Sci. Instrum. 82 (2011) 013708. doi:10.1063/1.3529919.

[52] Z. Ma, Q. Liu, H. Liu, H. Yang, J.X. Yun, M. Xu, C.A. Eisenberg, T.K. Borg, R. Markwald, B.Z. Gao, Cardiogenic Regulation of Stem-Cell Electrical Properties in a Laser-Patterned Biochip, Cell. Mol. Bioeng. 5 (2012) 327–336. doi:10.1007/s12195-012-0240-0.

[53] S. Zhang, L. Yan, M. Altman, M. Lässle, H. Nugent, F. Frankel, D.A. Lauffenburger, G.M. Whitesides, A. Rich, Biological surface engineering: a simple system for cell pattern formation, Biomaterials. 20 (1999) 1213–1220. doi:10.1016/S0142-9612(99)00014-9.

[54] C.A. Scotchford, C.P. Gilmore, E. Cooper, G.J. Leggett, S. Downes, Protein adsorption and human osteoblast-like cell attachment and growth on alkylthiol on gold self-assembled monolayers, J. Biomed. Mater. Res. 59 (2002) 84–99. doi:10.1002/jbm.1220.

[55] M.C. Jo, R. Guldiken, A label-free cell separation using surface acoustic waves, in: 2011 Annu. Int. Conf. IEEE Eng. Med. Biol. Soc., IEEE, 2011: pp. 7691–7694. doi:10.1109/IEMBS.2011.6091895.

[56] B. Hammarström, M. Evander, H. Barbeau, M. Bruzelius, J. Larsson, T. Laurell, J. Nilsson, Non-contact acoustic cell trapping in disposable glass capillaries, Lab Chip. 10 (2010) 2251. doi:10.1039/c004504g.